DOI: 10.6060/mhc235102z

Surface Properties, Interface Events and Energy Relaxation Processes in Nanoassemblies Based on Ag-In-S/ZnS Quantum Dots and Porphyrins

Eduard I. Zenkevich,[a,b@] Vladimir B. Sheinin,[c] Olga M. Kulikova,[c] and Oscar I. Koifman[c]

[a]*Belarussian National Technical University, 220013 Minsk, Belarus*
[b]*Chemnitz University of Technology, Research Center for Materials, Architectures and Integration of Nanomembranes (MAIN), 09107 Chemnitz, Germany*
[c]*G.A. Krestov Institute of Solution Chemistry, Russian Academy of Sciences, 153045 Ivanovo, Russia*
[@]*Corresponding author E-mail: zenkev@tut.by*

Based on comparative experimental spectral-kinetic data and quantum chemical calculations (method MM+) it was argued that in water at pH 7.5 and ambient temperature, electrostatic interactions of positively charged 5,10,15,20-tetra(N-methyl-4-pyridyl)porphyrin molecules (free bases) with negatively charged glutathione stabilized core/shell semiconductor quantum dots (QD) AIS/ZnS/GSH lead to the formation of stable «QD-porphyrin» nanoassemblies. The obtained results indicate that interaction of AIS/ZnS/GSH QDs with positively charged H_2P^{4+} molecules is not described appropriately by the Poisson statistics (the nanoassembly stoichiometry is 1:1), and followed by a very fast metalation of porphyrin free base (formation of the extra-ligated Zn-porphyrin complex) which is directly fixed on the QD surface. The detailed analysis of experimental results and structural parameters for the size-consistent 3D model of the above «QD-porphyrin» nanoassembly evidently showed for the first time that the non-radiative relaxation of QD excitonic excitation energy is due to competitive processes: FRET QD → porphyrin and the electron tunneling through the ZnS barrier to the outer interface of the QD in conditions of quantum confinement.

Keywords: Core/shell semiconductor quantum dots, glutathione stabilization, tetrapyridyl substituted porphyrins, "quantum dot – porphyrin" nanoassemblies, electrostatic interactions, quantum chemical modeling (MM+), quantum dot surface morphology, steady state spectroscopy, time-resolved spectroscopy, quantum dot photoluminescence quenching, Foerster resonance energy transfer model (FRET), electron tunnelling, quantum confinement.

Поверхностные свойства, интерфейсные явления и процессы релаксации энергии в наноансамблях на основе полупроводниковых квантовых точек Ag-In-S/ZnS и молекул порфиринов

Э. И. Зенькевич,[a,b@] В. Б. Шейнин,[c] О. М. Куликова,[c] О. И. Койфман[c]

[a]*Белорусский национальный технический университет, 220013 Минск, Беларусь*
[b]*Технический университет Хемнитца, Центр исследования материалов, архитектур и интегрирования наномембран (МАИН), D-09107 Хемнитц, Германия*
[c]*Институт химии растворов им. Г.А. Крестова РАН, 153045 Иваново, Россия*
[@]*E-mail: zenkev@tut.by*

На основании сравнительных спектрально-кинетических данных и квантово-химических расчетов (метод ММ+) обосновано, что в воде при pH 7.5 и комнатной температуре электростатические взаимодействия положительно заряженных молекул 5,10,15,20-тетра(N-метил-4-пиридил)порфирина (свободные основания) с отрицательно заряженными стабилизированными глютатионом полупроводниковыми квантовыми точками (КТ) AIS/ZnS/GSH приводит к формированию стабильных наноансамблей «КТ-порфирин». Полученные результаты показывают, что взаимодействие КТ AIS/ZnS/GSH с положительно заряженными молекулами H_2P^{4+} не описываются статистикой Пуассона (стехиометрия наноансамблей 1:1) и сопровождается очень быстрой металлизацией молекулы свободного основания порфирина (образование экстра-лигандированного комплекса Zn-порфирина), которая непосредственно фиксируется на поверхности КТ. Детальный анализ

экспериментальных результатов и структурных параметров размерно-согласующейся 3D модели наноансамбля «КТ-порфирин» впервые показал, что безызлучательная релаксация энергии экситонного возбуждения КТ обусловлена двумя конкурирующими процессами: ферстеровским переносом энергии КТ → порфирин и туннелированием электрона сквозь барьер ZnS на внешнюю поверхность КТ в условиях квантового ограничения.

Ключевые слова: Полупроводниковые квантовые точки, стабилизация глютатионом, тетрапиридилзамещенные порфирины, наноансамбли «квантовая точка-порфирин», электростатические взаимодействия, квантово-химическое моделирование (ММ+), морфология поверхности квантовой точки, стационарная спектроскопия, время-разрешенная спектроскопия, тушение фотолюминесценции квантовых точек, модель Ферстера индуктивно-резонансного переноса энергии (FRET), туннелирование электрона, квантовое ограничение.

Introduction

It is well-documented that supramolecular functional arrays represent an emerging class of materials that have been governed by the supramolecular chemistry of molecules and supramolecular nanoassemblies via various noncovalent inter- and intramolecular forces through bottom-up assembly approaches.[1-8] Such high-order molecular hierarchies have been stabilized by various kinds of noncovalent intermolecular forces including hydrogen bonding, electrostatic, donor-acceptor, π-π stacking interactions, and dispersion forces. In its turn, these works have provided a sound basis for the development and the in-depth understanding of the structure property relationship of supramolecular functional materials, paving the way toward the discovery and exploration of a diverse array of supramolecular scaffolds for possible applications in nanotechnology.[9-14] There are several basic directions how one may manipulate the supramolecular nanoassemblies of organic/inorganic components through sophisticated organic synthesis and rational structural design.

Molecular self-assembly, namely the spontaneous or driven association of molecules, is the basis of many successful strategies to produce nano- and mesoscopic structures that adopt thermodynamic minima. The designed self-organization process, the information necessary for the process to take place, and the algorithm that the process follows, must be stored in the components, and must operative vie selective molecular interactions. The photophysical/photochemical study of self-organized systems is the subject of nanophotonics which plays a pivotal role in advancing nano/bio/info technology by creating new interfaces between multiple disciplines.[15] In this respect, multiporphyrin assemblies are of fundamental importance as models for mimicking and the detailed study of the energy/electron transfer processes taking place in the light-harvesting antenna complexes and the photosynthetic reaction centers *in vivo*. A lot of interesting and important results obtained in this field of supramolecular chemistry have been presented and discussed in literature.[16-24, and refs. herein] In addition, multiporphyrin arrays with controllable structures and energy/electron transfer properties are also under promising intensive study due to the relevance of their potential applications as man-made molecular nanodevices in the nascent field of molecular electronics, nanotechnology and biomedicine.[25-31]

The exploration of the utilization of transition metal-containing counterparts through coordination chemistry has led to the construction of unique molecular scaffolds of diverse geometry owing to the versatility of the coordination geometry and the coordination number with different metal centers interacting with organic components.[32-37] It was shown that the competing interplay of noncovalent interactions between self-assembled molecules have been crucial to the construction of the supramolecular functional materials. In particular, the noncovalent directional metal–metal and ligand–ligand (π–π) interactions represent a unique class of noncovalent interactions, usually associated with intriguing spectroscopic and luminescence properties. In this direction some principal results have been obtained also for nano-scale multicomponent metallo-organic frameworks, based on tetrapyrrolic compounds[14,29,31,36,37] and studied under leadership of Professor A.Yu. Tsivadze, full member of Russian Academy of Sciences whose 80th birthday was celebrated in January 2023.

The field of nanoscience and nanotechnology is extending the applications of physics, chemistry, biology, engineering and technology into various systems of nanoscale dimensions where optical, physical, photochemical, redox and magnetic properties become size-dependent. In this connection, semiconductor nanocrystals (often referred to as quantum dots, QD, with diameters of 2÷10 nm) represent the specific class of matter between atomic clusters and bulk materials with well-defined size-dependent photophysical properties caused by electron/hole quantum confinement.[38-40] Based on ideas of inorganic-organic platform, the combination of the two directions, that is the anchoring of functional organic molecules or molecular complexes to tuneable inorganic wide gap semiconductor colloidal QDs, is of considerable scientific and practical interest.[41,42] Recently, it was shown that the large variety of functional organic molecules (including tetrapyrroles of various classes[43-53]) allows a broad scenario for modification of QD optical properties as well as to study and control the energy relaxation pathways and their efficiency.

Over the last three decades, the synthetic pathways to prepare semiconductor-based nanoassemblies have vastly expanded and developed. These developments allowed the formation of various hybrid nanosystems composed of different material combinations. The specific material combination can dictate the physical, chemical, and optical properties of the resultant hybrid nanosystem. Typically, several approaches based on a bottom-up strategy have been applied to form QD-dye nanoassemblies in liquid solutions and polymeric matrices:[5,16,47,54] (i) blends of QD-dye moieties with variable blend morphology; (ii) the attachment of dye molecules to QDs via a simple intercalation into the QD capping ligand shell; (iii) the attachment of dye molecules to QD polymer or biopolymer covering shells via chemical bonds; (iv) electrostatic interactions; (v) the covalent attachment of a modified fluorophore to an appropriately functionalized QD, and (vi) a non-covalent

self-assembly via a whole set of functional anchoring groups in dye molecules. Thus, spontaneous self-assembly, which occurs as a result of the complementarity of superstructure components, is the real background for the formation of QD-based nanoassemblies with a wide range of possible fundamental and practical applications. In addition, upon a comprehensive analysis of the morphology and photophysical properties of organic-inorganic nanoassemblies as well as the dynamics, mechanisms and pathways of excitation energy relaxation in these nanoobjects some principal issues should be taken into account,[5,17,39,55-57] such as a higher surface-to-volume ratio (compared with the corresponding bulk semiconductor materials), dangling bonds and trap states (which may affect photoluminescence properties of QDs), specific surface/interface effects, *etc*. The most common tool used to study the interaction of capping ligands with QD surfaces and ligand-lattice interface is solution-phase nuclear magnetic resonance (NMR) spectroscopy,[58-60] thermogravimetric analysis,[61] calorimetry[62] and X-ray techniques.[63]

Correspondingly, it follows from above considerations that the detailed and quantitative analysis of dye-mediated excitation energy relaxation processes in QD-dye nanoassemblies should be done with taking into account all these reasons. It is also clear that available experimental approaches (such as steady-state and time/spatially-resolved spectroscopy, single nanoobject detection, light scattering measurements, AFM, TEM, *etc.*) present a solid basis for studying the spectral-kinetic properties of QD-dye (or QD-porphyrin) nanoassemblies and are useful for the verification of theoretical calculations. But none of these experimental methods allows sufficiently resolved visualization of the structure of the colloidal QD surface/interface and some details of attachment of the dye molecule to it, thus limiting the evaluation of necessary structure-spectral-energetic correlations in a lot of cases. In this respect it should be mentioned that various theoretical various approaches (EMA, TDDFT, *ab initio* DFT, MD, *etc*.) may predict that attached organic ligands cause (depending on their number and physico-chemical properties) surface reconstruction, dimensionality and interface engineering and modify electronic states and electron-phonon coupling in QD-dye nanoassemblies.[64-69] Nevertheless, this fruitful information is not sufficient to fully account for experimental findings observed for QD-dye nanoassemblies. Concluding, it is evident that the combination of various experimental approaches and theoretical modelling should be used to analyse the surface-energetic correlations in QD-dye nanoassemblies.

Keeping in mind these considerations, we studied nanoassemblies based on *n*-trioctylphosphine oxide- (TOPO) and amine-capped CdSe/ZnS QDs attached via coordination bond with tetra-mesopyridyl-substituted porphyrins (as well as with perylene bisimides) in solutions at 77–295 K.[5,17,29,31,40,43,44,50,53,64] From the experimental point of view, we used the combination of ensemble and single nanoassembly experiments (including time-resolved spectroscopy), while theoretical analysis was based on quantum-chemical and quantum-mechanical calculations. Such an approach showed the following: (i) attached porphyrin molecules lead to the formation of QD surface states (having energies in the forbidden zone), cause QD photoluminescence (PL) quenching and change blinking times; (ii) the low temperature surface transformation of the capping TOPO or amine shell (at $T_{phase} \approx 220–230$ K) depends on porphyrin attachment; (iii) QD PL quenching in QD-porphyrin nanoassemblies is caused by two main competitive processes – Foerster resonant energy transfer (FRET) QD→Dye (10–15%) and stronger non-FRET quenching caused by the electron tunneling to the surface traps in the conditions of quantum confinement.

Very recently we described the results of comparative experimental study (steady-state absorption/ photoluminescence, time-resolved experiments, Raman spectroscopy, dynamic light scattering) and quantum chemical calculations (method MM+) describing Coulomb electrostatic interactions of positively charged 5,10,15,20-(tetra-N-methyl-4-pyridyl)porphyrin molecules with negatively charged glutathione stabilized core/shell semiconductor quantum dots (QD) AgInS/ZnS leading to the formation of stable QD-porphyrin nanoassemblies in water (p*H* 7.5) at ambient temperature.[47,70-76] Using elaborated size-consistent quantum chemical atomistic 3D model for glutathione stabilized AgInS/ZnS QD, we analysed a detailed physico-chemical mechanism for the interaction of the porphyrin molecule with the QD including surface/interface effects surface taking place with both QD and porphyrin molecules. These results highlight the complexity of interface processes in "QDs – porphyrin" nano-assemblies and provide valuable strategies for the detailed analysis of the excitation energy relaxation in the systems under study. Here, taking into account these recent findings (including basic experimental results and theoretical calculations) we present the comprehensive analysis of the pathways and mechanisms for exciton relaxation processes (*e.g.* energy transfer and other competing channels) in AgInS/ZnS QD-porphyrin nanoassemblies.

Experimental

Functional porphyrin macrocycles. Positively charged 5,10,15,20-tetra(N-methyl-4-pyridyl)porphyrin tetraiodide, H_2P^{4+} and its Zn-complex, ZnP^{4+} were synthesized and purified according to methods described in literature.[77-81] For comparison, absorption and fluorescence spectra were analysed also for axial aqua Zn-complex, $(H_2O)ZnP^{4+}$ and Zn-porphyrin extra-coordinated with strong ligands $(L)ZnP^{4+}$ such as pyridine (Py), imidazole (Im) or anion (OH^-) in water at p*H* 7.5 and T=298 K. Chemical structures and absorption/fluorescence spectra of the corresponding individual porphyrins are presented in Figure 1. It was experimentally proven that in the concentration range $C = (3–30)\cdot10^{-5}$ M, all porphyrins (used in titration experiments) remain in monomeric form in water at p*H* 7.5 and T=298 K.[75] For H_2P^{4+} the following molar decimal extinction coefficients were used:[82] $\varepsilon_{422} = 2.2\cdot10^5$ $M^{-1}cm^{-1}$, $\varepsilon_{512} = 1.8\cdot10^4$ $M^{-1}cm^{-1}$ and $\varepsilon_{584} = 5.4\cdot10^3$ $M^{-1}cm^{-1}$. In the case of ZnP^{4+} molecules with various extra-ligands the corresponding values were taken into consideration: $\varepsilon_{563} = 1.5\cdot10^4$ $M^{-1}cm^{-1}$, $\varepsilon_{605} = 5.0\cdot10^3$ $M^{-1}cm^{-1}$.

Semiconductor quantum dots. Colloidal Ag-In-S/ZnS core/shell QDs stabilized by glutathione (GSH) as native ligand (AIS/ZnS/GSH QD, $d_{AIS/ZnS} \approx 2.5–3$ nm) were synthesized in water in a reaction between GSH complexes of Ag^I and In^{III} with sodium sulphide according to described procedures.[83-85] ZnS shell was deposited on the AIS cores by decomposition of the Zn(II)-GSH complex at 96-98 ºC (being in the excess in the solution). For AIS/ZnS/GSH QDs under study the following molar decimal extinction coefficients were used:[83-85] $\varepsilon_{320} = 6.7\cdot10^5$ $M^{-1}cm^{-1}$, $\varepsilon_{350} = = 4.8\cdot10^5$ $M^{-1}cm^{-1}$ and $\varepsilon_{400} = 2.9\cdot10^5$ $M^{-1}cm^{-1}$. Authors are especially grateful to Dr. A. Raievska and Dr. A. Stroyuk from Helmholtz Institute Erlangen-Nürnberg for Renewable Energy (Erlangen, Germany) for their qualified assistance in this part of the work. Schematic presentation of AIS/ZnS/GSH QD is shown in Figure 1.

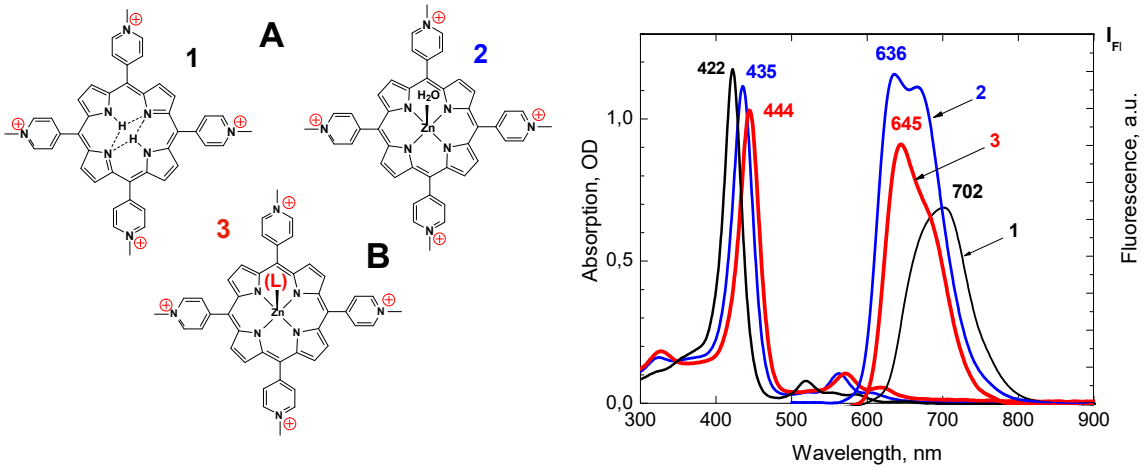

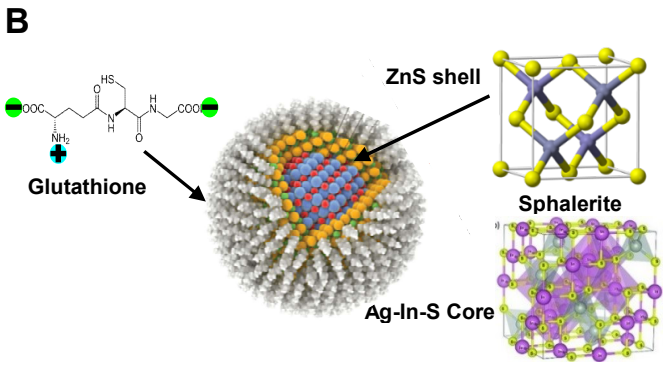

Figure 1. Structure and spectral properties of interacting subunits forming AIS/ZnS/GSH QD-porphyrin nanoassemblies. **A**: Chemical structures and absorption/fluorescent properties of positively charged porphyrins used for the study of their electrostatic interactions with negatively charged AIS/ZnS/GSH QDs during titration experiments in water solutions at p*H* 7.5 and T = 298 K: 1 (black) – positively charged 5,10,15,20-tetrakis(N-Me-pyridin-4'-yl) porphine tetracation, H_2P^{4+}; 2 (blue) – its axial aqua Zn-complex, $(H_2O)ZnP^{4+}$; 3 (red) – Zn-porphyrin extra-coordinated with strong ligands $(L)ZnP^{4+}$ such as pyridine (Py), imidazole (Im) or anion (OH^-). **B**: Schematic presentation of main components of AIS/ZnS/GSH QD, including Ag-In-S core (sphalerite structure[83-85]), ZnS shell and capping glutathione layer with negatively charged carboxylic groups interacting with positively charged N-methyl-pyridyl groups of the porphyrin free base molecule H_2P^{4+} via Coulomb forces.

QD-porphyrin nanoassemblies. The controllable formation of AIS/ZnS/GSH-porphyrin nanoassemblies, based on electrostatic interactions between negatively charged carboxylic groups of QD ligands (GSH) and positively charged N-methyl-pyridyl groups of H_2P^{4+} or $(H_2O)ZnP^{4+}$ molecules was realized during titration experiments in water solutions (p*H* 7.5, T = 298 K). Porphyrins were sequentially added in steps of 10 μL from a high concentrated stock solution (C_{porph} ~ $8\cdot10^{-6}$ – $3\cdot10^{-5}$ M) to the QD solution (V = 4 mL, C_{QD} = 0.5–$1.0\cdot10^{-6}$ M) up to wanted molar ratios x = $[H_2P]/[QD]$. The physico-chemical description of titration experiments has been presented in our earlier publications,[5,47,50,75,76,86,87] which contain also the detailed information on experimental methods and spectral-kinetic setup (UV-vis absorption, steady-state and time-resolved fluorescence measurements, Raman spectroscopy, dynamic light scattering, *etc*.).

Results and Discussion

With respect to the properties and reactivity of semiconductor QDs and QD-dye nanoassemblies, one of the most defining features is the QD surface/interface.[39,88-93] Compared to bulk semiconductors, QDs have much larger surface area-to-volume ratios. This results in a class of materials with properties that are heavily influenced by the structural and electronic character of the surface itself as well as capping ligand nature and by physico-chemical properties of attaching organic functional chromophores.[5,47,55,94-98] Nevertheless, as was mentioned in Introduction, despite their importance in dictating QD reactivity and properties, QD surfaces are poorly understood due to a lack of molecular-level information. In this respect functionalized organic molecules (including porphyrin macrocyles) may be used as specific probes for modifying and studying QD surface morphology, energy states, optical properties, and pathways of exciton relaxation.[5,29,47,55,75,76] With these considerations in mind, here we would like to quantitatively analyse the morphology as well as reasons and mechanisms of QD PL quenching in AIS/ZnS/GSH-porphyrin nanoassemblies examined in details recently.[47,70-76]

Spectral-kinetic properties of nanoassemblies. The main experimental findings are the following (Figures 2 and 3). Upon titration of QD solution by porphyrin free bases H_2P^{4+} the characteristic Soret and Q-bands in absorption appear on a top of the featureless QD absorption curve accompanied by a significant decrease of QD PL intensity without noticeable changes of PL maximum position and FWHM (Figure 2A,B). At every titration step the injection of H_2P^{4+} molecules into AIS/ZnS/GSH QDs solution leads to an immediate drop of PL intensity. Notably, during titration experiments upon nanoassembly formation the observed strong decrease of QD PL intensity (Figures 2B and 3A) does not lead to noticeable changes of QD PL decay curves (Figure 2C): QD mean multiexponential PL decay time of $\langle\tau\rangle \approx (350 \pm 20)$ ns remains the same in the whole titration range. From the basic physico-chemical background, the reason of the observed QD PL quenching in nanoassemblies under study may be caused by both "dynamic" and "static" quenching mechanisms,[5,99] For the given nanoassemblies, the corresponding quantitative consideration of this quenching based on a developed size-proportional atomistic 3D model of the AIS/ZnS/GSH QD and porphyrin ligands will be given below.

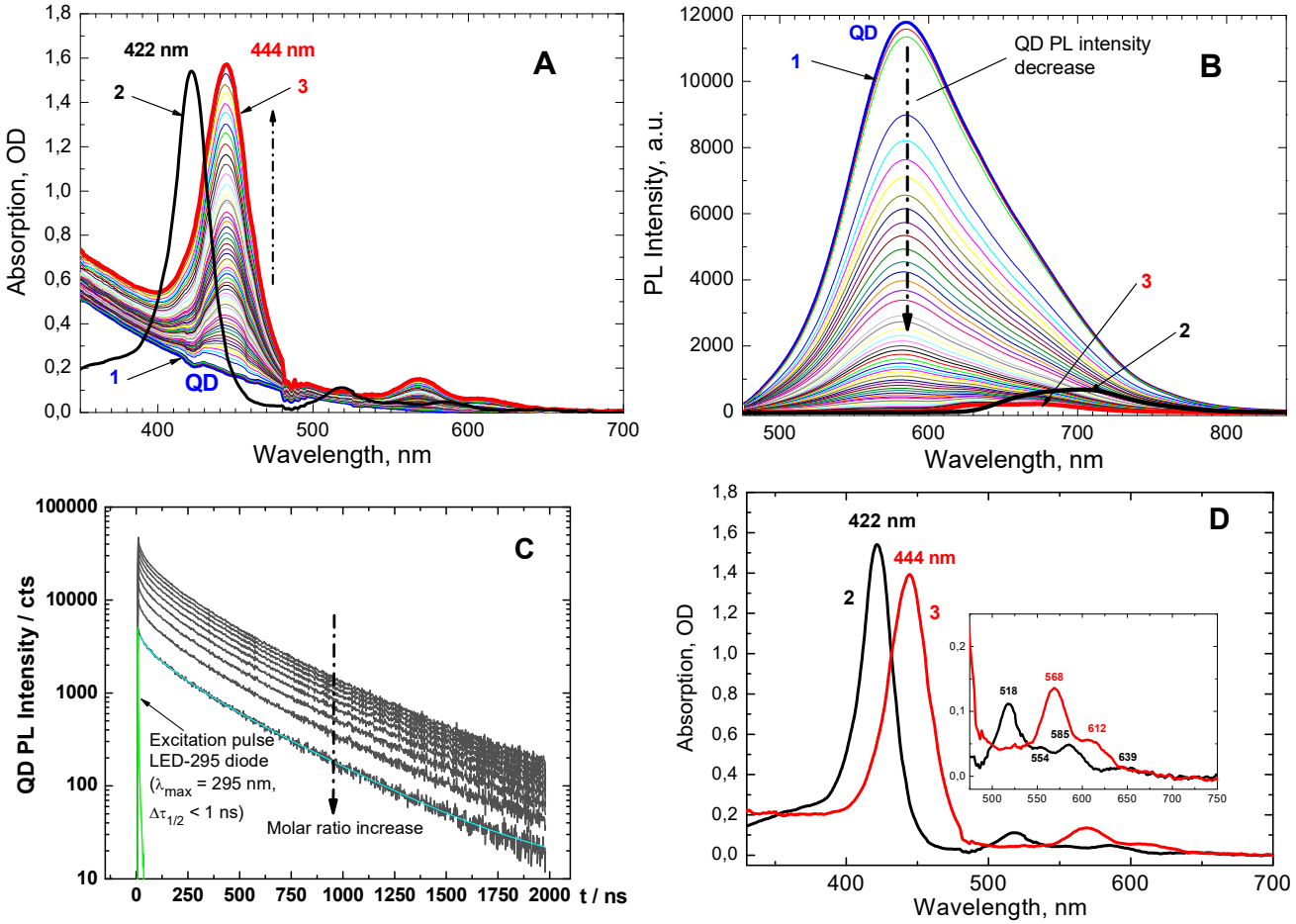

Figure 2. Titration of AIS/ZnS/GSH QD solution by increasing quantity of porphyrin free base H_2P^{4+} molecules (upon the molar ratio x = [Porphyrin]/[QD] increase) in water at 298 K and p*H* 7.5. **A:** Absorption spectra: 1 (blue) - alone QD; 2 (black) – absorption spectrum of alone porphyrin free base H_2P^{4+}; 3 (red) – absorption spectrum of porphyrin attached to QD at the final titration step ($x \geq 1$). Vertical arrow shows the increase of the absorbance of porphyrin added to QD solution during titration steps, concentrations of **2** and **3** are the same. **B**: Photoluminescence (PL) spectra (λ_{ex} = 300 nm): 1 (blue) - alone QD, vertical arrow shows the decrease of QD PL intensity after sequential addition of H_2P^{4+} molecules; 2 (black) – fluorescence spectrum of alone porphyrin free base H_2P^{4+}; 3 (red) – fluorescence spectrum of porphyrin attached to QD at the final titration step ($x \geq 1$), concentrations of **2** and **3** are the same. **C**: QD PL decay curves (λ_{ex} = 295 nm, λ_{det} = 585 nm) upon sequential addition of H_2P^{4+} molecules. **D**: Absorption spectra of alone H_2P^{4+} (2, black) and porphyrin molecules attached to AIS/ZnS/GSH QD (3, red) measured at the final titration step ($x \geq 1$), concentrations of **2** and **3** are the same.

Figure 2D shows also that, in contrast to nanoassemblies of CdSe/ZnS QDs and tetra-*meso*-pyridyl substituted porphyrin free bases $H_2P(m\text{-}Pyr)_4$, where the spectral properties of attached porphyrins remained unchanged,[5,17,29,43,44,50,53] pronounced spectral transformations (both for Soret and Q-bands) are observed for porphyrin molecules electrostatically attached to AIS/ZnS/GSH QD surfaces with respect to the corresponding spectra for pure H_2P^{4+} molecules at the same concentrations and conditions. In particular, the porphyrin Soret band maximum is red shifted from 422 nm (detected for pure H_2P^{4+} molecules) to 444 nm for the attached porphyrin molecules accompanied by corresponding spectral changes in the range of Q-bands (inset in Figure 2D). A similarly pronounced effect is also observed in fluorescence spectra of porphyrin macrocycle upon attachment to AIS/ZnS/GSH QD (spectra 2 and 3, Figure 2B). It means that in latter case H_2P^{4+} molecules may be considered as a specific spectral probe for the study of some features of AIS/ZnS/GSH QD interface.

Recently, based on additional experimental studies (including Raman spectroscopy and some chemical procedures) together with the analysis of known absorption/fluorescence spectra of porphyrin free bases and corresponding metalloporphyrins, it was definitely shown,[75] that for porphyrin molecules electrostatically attached to the surface of glutathione stabilized AIS/ZnS/GSH QD the main absorption/fluorescence features correspond to those, which are typical for Zn-porphyrins. In fact, being electrostatically attached to the negatively charged glutathione GSH shell on the QD surface, H_2P^{4+} molecules may extract Zn^{2+} ions from GSH layer, thus forming ZnP^{4+}porphyrin, in which the central Zn ion is additionally coupled with the strong extra-ligand.

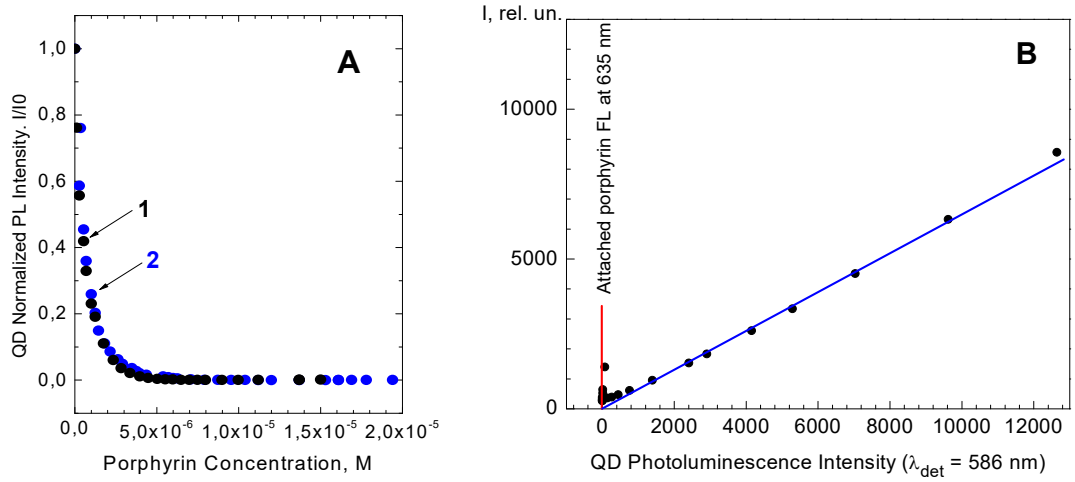

Figure 3. Photoluminescence properties of nanoassemblies. **A**: Dependence of normalized PL intensity of AIS/ZnS/GSH QDs on porphyrin concentration upon titration by positively charged porphyrin H_2P^{4+} (1, black, structure **1** in Figure 1A) and axial aqua Zn-complex $(H_2O)ZnP^{4+}$ (2, blue, structure **2** in Figure 1A) in water, p*H* 7.5, T = 298 K (λ_{exc} = 380 nm). **B**: Correlation measurements for the analysis of full PL quenching for solution of AIS/ZnS/GSH QDs upon titration by H_2P^{4+}. Correlation dependence for full PL quenching for AIS/ZnS/GSH QDs (λ_{reg} = 586 nm) accompanied by the appearance of fluorescence emission of extra-ligated ZnP^{4+} molecule attached to the QD surface. Based on procedure described in[100] the limit of detection was calculated as $1.98 \cdot 10^{-4}$.

Formation and surface morphology of AIS/ZnS/GSH QD - porphyrin nanoassemblies. At the moment, none of the experimental methods allows sufficiently resolved visualization of the processes realized upon attachment of the dye molecule (porphyrins in our case) on the colloidal QD surface. To gain molecular-level understanding of the QD surface and its interaction with functional organic chromophores, the structure and physico-chemical peculiarities must be determined for each of these three coupled components: the inorganic crystal lattice, the ligand shell organization and chromophore attachment. Several fundamental properties play the basic role in this case: structure formation and reactivity of the inorganic lattice and interface: the material crystal structure, the exposed facets, QD shape (morphology) and interface effects caused by capping ligand and attached functional molecules. Basically,[39,67,69,88] these properties result from energy minimization of the surface during QD synthesis as well as upon interaction with functional organic molecules.

A deeper insight into the interface properties and energy relaxation processes realized in nanoassemblies based on AIS/ZnS/GSH QDs electrostatically coupled with porphyrin macrocycles occurs to be possible using a size-proportional 3D model elaborated by us[75,76] and based on available crystal structure information for Ag-In-S core (sphalerite zinc blende structure[83-85]), size of AIS/ZnS QD ($d_{AIS/ZnS} \approx 2.5$–3 nm[83-85]), and obtained experimental data. Not wishing to present here the whole description of our approach, we would like to highlight briefly some general basics of this model and its implication for the experimental data obtained for QD-porphyrin nanoassemblies under consideration. The construction of the atomistic scale model of AIS/ZnS/GSH QD is based on the quantum chemistry method MM+ which employs parametrized, classical representations of the interactions, using relatively simple approximations for potential, such as harmonic springs to describe bonds and valence angles as well as Coulomb and Lennard-Jones interactions to account for charge-charge and non-bonded contributions, respectively.[101,102] Correspondingly, an octahedral sphalerite nanocrystal $Zn_{161}S_{161}$ (diameter 2.7 nm) with a hydrolyzed $(SH)_{78}(ZnOH)_{78}$ surface solubilized by 24 glutathione molecules was constructed as an appropriate QD model. Then the final model of water-soluble $Zn_{161}S_{161}/(OH_{54}H_{78}(GS^-)_{24}$ quantum dot was obtained by the substitution of 24 surface hydroxo groups with ionized glutathione through a thiolate anchor SH group, resulting in a diameter of ~4.5 nm (Figure 4). The given model corresponds to a net filling of 31% facets ($ZnOH_{21}$,$ZnOH_{21}$, $ZnOH_{21}$,$ZnOH_{15}$), while the other four facets (SH_{21},SH_{21}, SH_{21},SH_{15}) remain free. Like it was discussed recently,[67,68] this means that the surface of AIS/ZnS/GSH QD in water is not homogeneous, Thus the given AIS/ZnS/GSH QD of this size cannot be considered as a "dandelion" model frequently used to depicture the QD surface covered by ligands.

According to the elaborated model, the formation of AIS/ZnS/GSH QD – porphyrin nanoassemblies is realized via electrostatic interactions of negatively charged carboxylic groups of capping GSH) layer and positively charged N-methyl-pyridyl groups of H_2P^{4+} or $(H_2O)ZnP^{4+}$ molecules, and takes place in three sequential and fast stages.[75,76] At the first stage, the diffusion-controlled formation of the electrostatic nanoassembly QD - H_2P^{4+} (1:1) takes place. Then, at the second stage, being electrostatically coupled with the negatively charged GSH layer on the QD surface, the positive H_2P^{4+} molecule extracts Zn^{2+} ion from GSH capping ligand shell (having Zn^{2+} ions during the synthesis of these QDs), and the formation of QD - ZnP^{4+} conjugate takes place where tetracation ZnP^{4+} may exist also as axial aqua Zn-complex, like $(H_2O)ZnP^{4+}$. At the third stage, aqua-complex of tetracation ZnP^{4+} quickly finds an open SH facet of AIS/ZnS/GSH QD and attaches via chemisorption on its surface, forming QD - $(L)ZnP^{4+}$ conjugate where central Zn ion in the porphyrin macrocycle is extra-coordinated with a strong ligand (via axial coordination bond ($\equiv S^-$)-ZnP^{4+}). The latter two stages proceed irreversibly and very fast, just at the moment of the titrant addition.

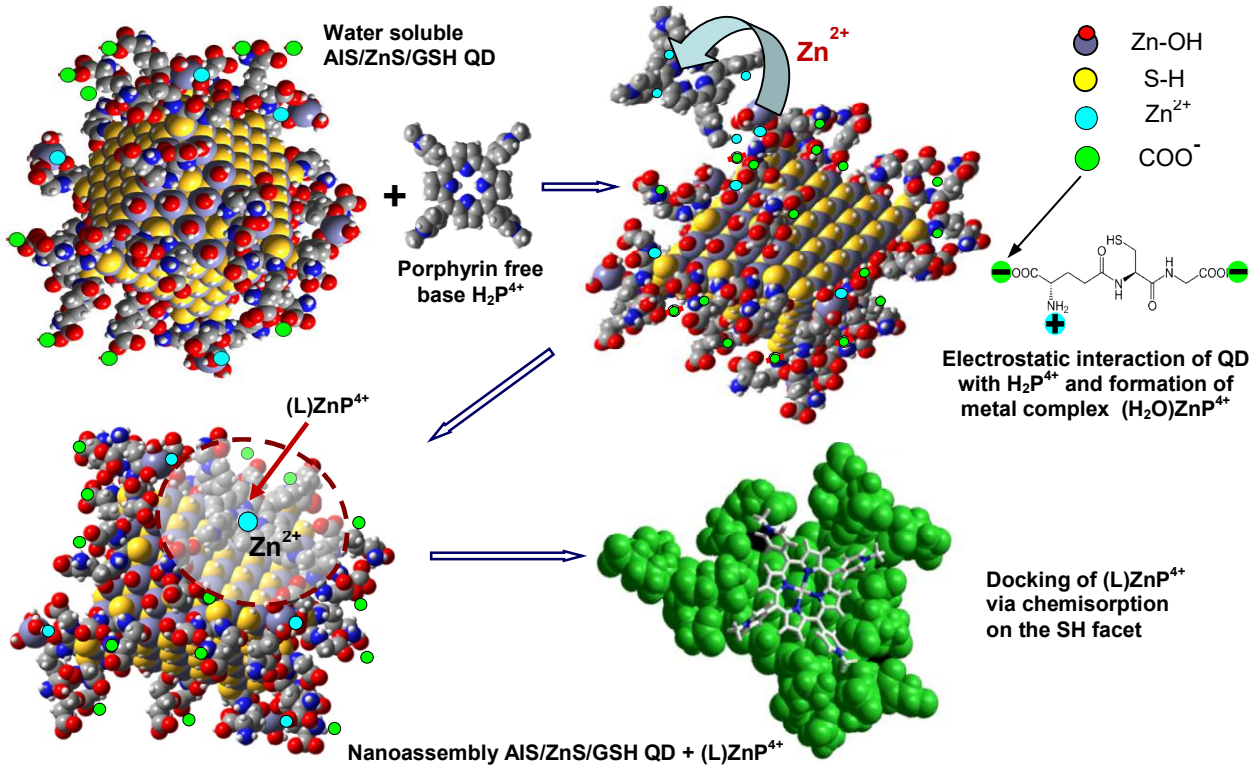

Figure 4. Formation of water-soluble AIS/ZnS/GSH QD–porphyrin nanoassemblies based on MM+ calculations. Total surface negative charge for the final water-soluble $Zn_{161}S_{161}/((OH)_{54}H_{78}(GS^-)_{24}$ QD (d = 4.5 nm) is determined by the difference between negative charges of GS-ligands and associated cations Zn^{2+}. The structure of porphyrin free base H_2P^{4+} (d = 1.85 nm) was calculated by DFTB3LYP/ 6-31++G(dp) method. Nanoassembly AIS/ZnS/GSH QD – $(L)ZnP^{4+}$ is formed via electrostatic interactions of negatively charged QD and positively charged H_2P^{4+} molecule followed by the metal (Zn) exchange process and sequential chemisorption of the porphyrin ZnP^{4+} molecule on empty (SH) facet of QD leading to the face-to-face axial complex (1:1) stabilization.

Our model shows that the formation of the QD - $(L)ZnP^{4+}$ nanoassembly is finished by electrostatic bonding of the peripheral cationic groups -Py^+Me with the carboxylate groups of conformationally mobile glutathione ligands, which adapt to the "guest" geometry. In this case, absorption of the QD - $(L)ZnP^{4+}$ nanoassembly (1:1) is a superposition of initial spectrum of AIS/ZnS/GSH QD and one belonging to the axial acid complex $(\equiv S^-)$-ZnP^{4+} (red shift of Soret band from 422 nm to 444 nm, see Figure 2A), lying on the surface of SH facet. After electrostatic coupling and metalation, the aqua complex $(H_2O)ZnP^{4+}$ gets readily chemisorbed on a S-terminated (SH) surface of AIS/ZnS/GSH QD resulting in the formation of the final nanoassembly AIS/ZnS/GSH QD - $(L)ZnP^{4+}$ (Figure 4). The possibility of alternative thiolate complex forming with glutathione-ligand was rejected by a negative test for the interaction of $(H_2O)ZnP^{4+}$ with an excess of free glutathione in aqueous solution where no spectral forms of ZnP^{4+} with the strong extra-ligand (λ_{Soret} = 444 nm) was observed.[75]

Nanoassembly composition and stability. Taking into account quantitative titration experiments for AIS/ZnS/GSH QDs of given sizes and structure, our model predicts the formation of 1:1 face-to-face QD-porphyrin nanoassembly, with planar ZnP^{4+} porphyrin lying on a SH-edge surface like a «pancake on a pan» as the most probable geometry (Figure 4). Nevertheless, this conclusion should be proven by some additional considerations and experiments. Basically, for a quantitative analysis of QD-porphyrin composition and reasons of QD PL quenching in nanoassemblies it is necessary to estimate of both the number of surface-attached molecules per QD and such molecules remaining in the solution using the so-called Poisson distribution.[50,53,97,103-106] This distribution describes the statistics of uncorrelated adsorption of functional molecules to QD surfaces taking into account the following items: (i) the mean number of surface-bound ligands is far from the number needed to saturate the QD surface, and (ii) there is a sufficiently large number of surface sites (Figure 5).

It should be noted in this respect that in a lot of cases the Poisson distribution is silently used without the corresponding arguments for its application though such an analysis should be done, at least. The corresponding analysis was carried out by us for nanoassemblies based on coordination interactions of trioctylphosphine oxide (TOPO)-capped CdSe/ZnS QDs and tetra-pyridyl porphyrins.[50,53,97,106] It was experimentally shown that the attachment of functional porphyrin molecules to the QD surface is realized in the competition (like dynamic equilibrium) with TOPO molecules, and thus the ligand exchange of the native TOPO ligands of CdSe/ZnS QDs by porphyrins is not a simple first-order process. In this case, the maximum number (n_{max}) of attached H_2P molecules depends on several factors (*e.g.*, the number and kind of non-dependent accessible places on the QD surface which

are not occupied by TOPO molecules, complexation constants for TOPO and H_2P depending on the solvent nature and their relative concentrations, *etc*.). On the basis of these findings it was concluded that the formation of nanoassemblies based on TOPO-capped CdSe/ZnS QDs and tetra-pyridyl porphyrins in toluene at ambient temperature does not obey the Poisson statistics.

Correspondingly, the problem thus presented seems to be analysed also for nanoassemblies based on AIS/ZnS/GSH QDs with electrostatically attached positively charged porphyrin free bases H_2P^{4+}. It follows from the size-consistent 3D-model of the given QD,[75,76] that only limited number of porphyrin molecules may be fixed directly to the QD surface facets (SH_{21},SH_{21},SH_{21},SH_{15}) in order to form a stable complex, and the maximal valid value is n=4 per landing pad number (see Figure 4). Nevertheless, the analysis of experimental results on the dynamic light scattering (estimations of as Z-potential and size of AIS/ZnS/GSH QDs and QD-porphyrin nanoassemblies) indicates,[75,76] that the reasonable stoichiometry is 1:1 for the stable nanoassembly of negatively charged AIS/ZnS/GSH QD with positively charged porphyrin molecule. This conclusion is also supported by results of comparative titration experiments:[75] titration of AIS/ZnS/GSH QDs by H_2P^{4+} molecules (Figure 2A,B,D), by added amounts of $(H_2O)ZnP^{4+}$ molecules, and reverse titration of H_2P^{4+} solution by AIS/ZnS/GSH QDs show that in all these three cases at molar ratio 1:1 (in the case of QD PL full quenching) spectral properties of attached porphyrin molecule in AIS/ZnS/GSH QD-porphyrin nanoassembly correspond to metalloporphyrin ZnP^{4+} with strong extra-ligand L (Soret band maximum at λ_{Soret} =444 nm). At the final titration stage (molar ratio $x = [C_{porphyrin}]/[C_{QD}] = 1$) the attached porphyrin $(L)ZnP^{4+}$ may not be free base (λ_{Soret} = 422 nm) or aqua Zn-complex $(H_2O)ZnP^{4+}$(λ_{Soret} = 436 nm).

It follows from the 3D-model of QD that, in principle, the second porphyrin molecule may be electrostatically attached to GSH shell of AIS/ZnS/GSH QD and may be detected as an additional aqua Zn-complex $(H_2O)ZnP^{4+}$ (λ_{Soret} = 436 nm). With this idea in mind, we carried out the titration of solution with formed nanoassembly AIS/ZnS/GSH QD + $(L)ZnP^{4+}$(1:1) by H_2P^{4+} molecules up to the molar ratio $x = C_{porph}/C_{QD}$ = 2:1 (the detailed information will be presented in separate publication). It was found that upon increasing x >1 the non-stability is observed for the colloid solution of nanoassemblies. After reaching the molar ratio $x = C_{porph}/C_{QD}$ = 2:1 the collapse of this three-component complex $(L)ZnP^{4+}$[AIS/ZnS/GSH QD]&$(H_2O)ZnP^{4+}$ takes place. This complex gradually decomposes into an insoluble component $(L)ZnP^{4+}QD$, which completely precipitates, and aqua Zn-complex $(H_2O)ZnP^{4+}$, which remains in solution. It may be explained by the fact, that the stability of colloid nanoassemblies depends on the total surface charge which is determined by the difference of the negative charges GS^- of ligand glutathione molecules and coupled with them associated cations Zn^{2+}. Thus at $x = C_{porph}/C_{QD}$ = 2:1, the charge compensation takes place (due to the second attached positively charged porphyrin molecule), which results in the formation of an unstable colloidal phase followed by the precipitation process. Correspondingly, taking into account all these results and given argumentation one may conclude that interaction of AIS/ZnS/GSH QDs with positively charged H_2P^{4+} molecules is not described appropriately by the Poisson statistics, and the most probable stoichiometry of the nanoassembly AIS/ZnS/GSH QD + $(L)ZnP^{4+}$ is 1:1. The formation of stable nanoassemblies containing one AIS/ZnS/GSH QD and two or even more porphyrin molecules is low probable in water at p*H* 7.5 and ambient temperature.

Finally, the formation of multicomponent chains like $[\text{-QD-Porphyrin-QD-Porphyrin-QD-}]_n$ is impossible due to the electrostatic repulsion of neighbouring glutathione capped negatively charged AIS/ZnS/GSH QDs, which is stronger essentially compared to the electrostatic attraction of a positively charged porphyrin macrocycle ZnP^{4+} (having a small positive charge and attached to one AIS/ZnS/GSH QD) with the second negatively charged QD.

$$P(n,x) = x^n \cdot \frac{exp(-x)}{n!} \quad (1)$$

$x = [C_{porphyrin}]/[C_{QD}]$ is given molar ratio
$n = 0 \div \infty$ is the number of attached molecules to the QD surface.

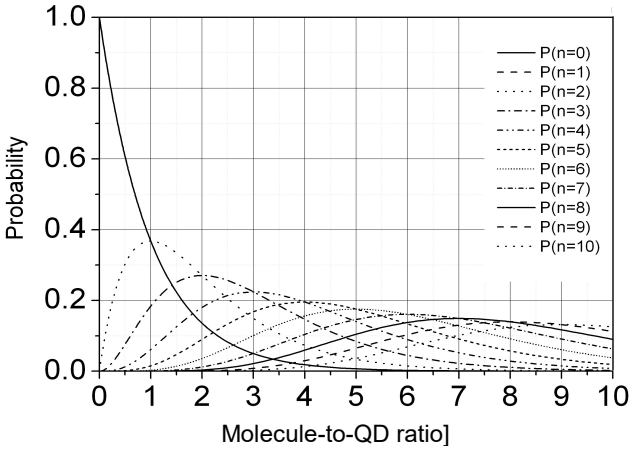

Figure 5. Poisson statistics for the probability P(n, x) to find n dye molecules (number n) fixed on the QD surface at a given molar ratio (x). Equation (1) holds in the case when the complexation constant K (describing the QD-dye interaction) is infinitely large, which implies that one does not have to consider a dynamic equilibrium.

A quantitative analysis of the excitation energy relaxation pathways in nanoassemblies. Experimental results presented in Figures 2 and 3 evidently show that the formation of AIS/ZnS/GSH QD – porphyrin nanoassemblies manifests itself in a strong quenching of the QD PL without any modifications of the maximum position and spectral line shape of the QD PL band. This PL quenching is not accompanied by noticeable changes of QD PL decay. In addition, at the final titration step at molar ratio $x \geq 1$ (when QD PL is fully quenched), fluorescence properties (the position in the energy scale and the spectral form) of the attached strongly ligated porphyrin molecule (L)ZnP^{4+} do not depend on the excitation wavelength. It means that the formation of the emitting state (belonging exclusively to the porphyrin subunit in nanoassemblies under study) occurs within very short (probably, ps) timescale. Nevertheless, it is known[5,51,53,107-109] that the quenching of QD PL by surface trap states of various nature in QD-dye nanoassemblies may be also rather quick thus competing with the non-radiative population of the acceptor excited state (*e.g.* Zn-porphyrin excited S_1-state in AIS/ZnS/GSH QD - **(**L)ZnP^{4+} nanoassembly).

It is seen from Figure 2 that at molar ratio $x \geq 1$ QD PL (with λ_{max} = 588 nm) is fully quenched, and one can detect fluorescence bands of extra-ligated ZnP^{4+} molecules electrostatically coupled to QD surface (red curve 3). It was found also[75] that at the same concentrations, the fluorescence relative intensity of ZnP^{4+} molecules electrostatically coupled to QD surface is lower than that found for alone axial aqua Zn-complex $(H_2O)ZnP^{4+}$. It follows from these results that extra-ligated ZnP^{4+} molecules coupled to QD surface, forming a strong axial coordination bond ($\equiv S^-$)-ZnP^{4+} between zinc ion in ZnP^{4+} and surface sulphur atom) possess measurable fluorescence. The reason of the lower fluorescence quantum yield for coupled ZnP^{4+} molecules compared to alone $(H_2O)ZnP^{4+}$ molecules in water solution may be explained by the following way. Typically[17,110,111] in various solvents for the most monomeric Zn-porphyrin complexes fluorescence lifetimes are $\tau \sim$ 1-2 ns and quantum yields are $\varphi \sim$2-3%. The τ shortening and φ lowering compared to these values measured for the corresponding porphyrin free bases is due to the increase of the non-radiative intersystem crossing $S_1 \sim\!\!> T_1$ processes in Zn-complexes[112,113] In some cases,[111,112] the formation of a mono-liganded form of Zn-porphyrin molecule leads to a distortion of a Zn-porphyrin macrocycle followed by an increase of the non-radiative deactivation of excited singlet and triplet states due to the electron-excitation energy exchange and the enhancement of a spin-orbital coupling as a result of the disturbance of the planarity of a macrocycle.

With respect to nanoassemblies under study, the interaction of attached ZnP^{4+} molecules with sulphur facet surface of QD via a formation of a strong axial coordination bond ($\equiv S^-$)-ZnP^{4+} may cause an additional distortion of Zn-porphyrin plane, thus leading to a stronger quenching influence in this case compared to alone $(H_2O)ZnP^{4+}$ molecules in water. Based on a relatively low intrinsic fluorescence quantum yields and very short fluorescence lifetimes of Zn-porphyrins in comparison with corresponding values of AIS/ZnS/GSH QDs ($\langle\tau\rangle \approx$ (350 ns, $\varphi \approx$ 40-60%[83-85,75,76]) the emission of ZnP^{4+} molecules being electrostatically coupled to the QD surface becomes observable only when the QD PL is strongly quenched in self-assembled arrays. Thus, as the Zn-porphyrin fluorescence is not drastically diminished upon attachment to QD surface compared to alone axial aqua Zn-complex $(H_2O)ZnP^{4+}$ in water, all these findings may be considered as the background to exclude the manifestation of charge transfer processes, and consider ZnP^{4+} molecules as potential acceptors of the excitation energy from excited AIS/ZnS/GSH QDs.

From photophysical background, the observed PL quenching for AIS/ZnS/GSH QD in nanoassemblies may be interpreted as being due to the photoinduced charge (electron or hole) transfer[114-116] and/or Förster resonance energy transfer (FRET)[117,118] from the QD to the attached porphyrin molecule. But it should be emphasized in this respect, that the detection of the fluorescence of porphyrin molecules electrostatically coupled to QD in nanoassemblies under study (see Figure 2, curve 3) is a strong argument to describe the QD PL quenching as a result of (fast and effective) FRET QD $\rightarrow$ (L)ZnP^{4+}. Otherwise, according to Marcus theory[114] in case of charge transfer process the emission of both donor and acceptor of charge is supposed to be quenched significantly.

To date, there have been carried out numerous studies of FRET from QDs to various acceptor organic ligands including experimental approach[5,29,41,44,50,52,97,107-109,119-125] and theoretical considerations.[64,126,127] It follows from these results that nanocrystalline materials and heterogeneous organic-inorganic nanostructures are best described in the weak coupling regime. The application of the weak coupling model arises due to the dissimilarity in the wave functions of the molecular orbitals in organic systems and band-like orbitals in QDs that prevents traditional strong interactions. This allows the application of Förster model for FRET process, which is typically used at the limit of "localized oscillators" as a result of the electric dipole approximation.[5,15,105,117,118,124,126,127] Nevertheless, there are several key questions which should be taken into account upon quantitative analysis of FRET events in QD-dye nanoassemblies: i) whether QDs may be considered as point dipoles, ii) statistical distribution of dye molecules on the QD surface and how dye molecules are attached to it (rigidly of with free rotation), and (iii) how to account for multiple dye molecules being adsorbed to a single QD. Thus, keeping in mind these ideas we are able to study FRET in AIS/ZnS/GSH QD - **(**L)ZnP^{4+} nanoassemblies using both the obtained experimental data and basic information derived from elaborated size-consistent 3D-model.

With respect to QDs, one remark should be highlighted: FRET considerations make sense if the other non-radiative channels for QD PL quenching are vanishing. In this case, according to Förster model (phase incoherent weak coupling through the dipole-dipole interaction[121,122]) FRET from a photoexcited QD (*D*, donor) to a lower-energy organic acceptor (*A*, porphyrin) takes place due to the coupling of the dipole moment ($\boldsymbol{\mu}$) of an exciton in QD with absorbing transition (dipole moment) in nearby porphyrin chromophore. The application of Förster theory relies on the approximation that the distance R_{DA} between interacting *D* and *A* dipoles is larger than the length $|\boldsymbol{l}|$ of the transition dipoles themselves.

Based on approach described for CdSe/ZnS – porphyrin nanoassemblies in[50], the corresponding estimations may be obtained using well-known expressions[128] for oscillator strength f and transition dipole moment $|\boldsymbol{\mu}|$ of the corresponding low-energy excitonic / electronic transitions of interacting subunits:

$$f = 4.33 \cdot 10^{-9} \cdot \varepsilon_{max}(\nu)\Delta\nu_{1/2}\,, \qquad (2)$$

where $\varepsilon_{max}(\nu)$ is the molar decimal extinction coefficient in the maximum of the QD first excitonic absorption band, $\Delta\nu_{1/2}$ is the FWHM value of the corresponding band, and

$$f = (8\pi^2 m_e \nu|\boldsymbol{\mu}|^2) / 3he^2\,, \qquad (3)$$

where ν is transition frequency, m_e and e are electron mass and charge.

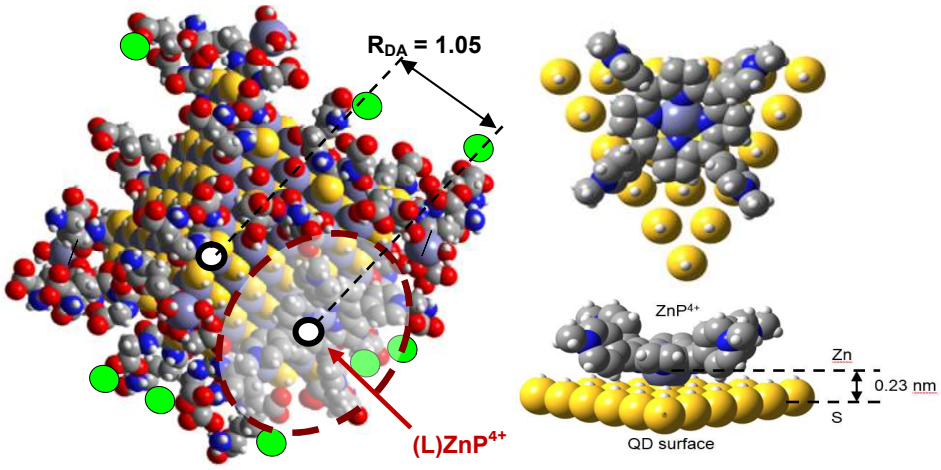

Figure 6. Arrangement of (L)ZnP^{4+} tetracation with respect to SH-facet surface of AIS/ZnS/GSH QD and estimated interplane distances between ZnP^{4+} molecule plane and SH-facet surface as well intercenter distance R_{DA} between QD and porphyrin macrocycle. Porphyrin plane is marked by a white ellipse.

Table 1. AIS/ZnS/GSH QD properties and parameters of FRET QD→(L)ZnP^{4+} in nanoassembly QD-porphyrin (water, T = 295 K, refractive index n = 1.333)

φ_D^{0} [a]	λ (nm)/ ε (10^3 $M^{-1}\cdot cm^{-1}$) [b]	$J(\nu)$ [c], 10^{-14} $cm^6\cdot M^{-1}$	R_0^{theor}, [d] Å	R_{DA}, Å	$\langle\tau_D^0\rangle$ [e], ns	k_{DA}, 10^9 s^{-1} (calculated)[f]
0.42±0.03	563 / 14.7·10^3 605 / 4.98·10^3	7.75	50.7	10.5	350±20	34.9

[a] φ_D^0 is the experimentally measured quantum yield of the photoluminescence of AIS/ZnS/GSH QD.
[b] Wavelength (λ) and the corresponding molar decimal extinction coefficient (ε) for absorption of the acceptor (L)ZnP^{4+}.
[c] $J(\nu)$ is the overlap integral between the donor (QD) emission and the acceptor (L)ZnP^{4+} absorption. The overlap integral is defined by[117,118] (see Figure 7):

$$J(\nu) = \int_0^\infty f_D(\nu)\varepsilon_A(\nu)\frac{d\nu}{\nu^4}\,, \qquad (4)$$

where $\varepsilon(\nu)$ corresponds to the molar decimal extinction absorption coefficient of the acceptor, $f_D(\nu)$ is the quantum PL emission spectrum of the donor normalized to unity by area on a wave number scale.
[d] The critical FRET radius R_0^{theor} was calculated as:[117,118]

$$\left(R_0^{theor}\right)^6 = \frac{9000\ln 10 k^2 \varphi_D^0}{128\pi^5 n^4 N_A} \times \int_0^\infty f_D(\nu)\varepsilon_A(\nu)\frac{d\nu}{\nu^4}\,, \qquad (5)$$

where $N_A = 6.022\cdot 10^{23}$ M^{-1} is Avogadro number, φ_D^0 is the D emission quantum efficiency in the absence of FRET, n is the refraction index of the solvent. Orientation factor $k^2 = [\mathrm{Cos}(\boldsymbol{\mu_D}, \boldsymbol{\mu_A}) - 3\,\mathrm{Cos}(\boldsymbol{\mu_D}, \mathbf{r_{DA}})\cdot \mathrm{Cos}(\boldsymbol{\mu_A}, \mathbf{r_{DA}})]^2$, where $(\boldsymbol{\mu_D}, \boldsymbol{\mu_A})$ is the angle between transition dipole moment vectors of the D and A subunits, $(\boldsymbol{\mu_D}, \mathbf{r_{DA}})$ and $(\boldsymbol{\mu_A}, \mathbf{r_{DA}})$ denote the angles between the dipole vectors of D and A and the direction D→A, respectively. For a random static rigid distribution of interacting dipoles $k^2 = = 0.476$.[50,118] This is the case for AIS/ZnS/GSH QD - (L)ZnP^{4+} nanoassemblies as far as few electronic and vibronic transitions of the porphyrin molecule overlap with a wide QD PL emission.
[e] $\langle\tau_D^0\rangle$ corresponds to PL mean decay of alone AIS/ZnS/GSH QD.
[f] FRET rate constant k_{DA} for the D-A pair was calculated as:[117,118]

$$\cdot k_{DA} = \frac{1}{\tau_D^0}\cdot\frac{R_0^6}{R_{DA}^6} \qquad (6)$$

Correspondingly, QD PL decay shortening is calculated by $\tau_D = 1/[(1/\tau_D^0) + k_{DA})]$. (7)

Molar decimal extinction coefficients $\varepsilon_Q \approx 4000–50000$ $M^{-1}cm^{-1}$ for Q-bands of porphyrins and Zn-porphyrins[43,50,77-82] (Table 1) correspond to an effective length of the transition dipoles $|l| \leq 1.1–1.3$ Å.[50] Using ε values for AIS/ZnS/GSH QDs in the region of the first excitonic transition[83-85] the correspondent values for transition dipole moment were estimated to be $|\mu| = 6.7–8.1$ Debye. Therefore, at one-electron excitation it gives an effective dipole length $|l| = 1.6–2.3$ Å. On the other hand, from the optimized geometry of the AIS/ZnS/GSH QD – $(L)ZnP^{4+}$ nanoassembly based on the elaborated size-consistent 3D model it follows that the intercenter *D-A* distance $R_{DA} = 10.5$ Å (Figure 6). It means that in this case the point dipole-dipole approximation is still valid which allows the application of Förster model to describe FRET.

Table 1 collects estimated parameters for FRET AIS/ZnS/GSH QD → $(L)ZnP^{4+}$ in nanoassemblies calculated within the framework of the dipole-dipole approximation on the basis of experimental data obtained in this study and theoretical expressions of Förster model. It follows from the data of Table 2 that FRET rate constant for the given D-A pair is estimated to be $k_{DA} = 34.9 \cdot 10^9$ s^{-1}, thus the characteristic transfer time should be $t_{FRET} = 1/k_{DA} = 2.9 \cdot 10^{-11}$ s = 29 ps. In the result, the following situation takes place: $<\tau_D^0>$ (350 ns) >> t_{FRET} (29 ps) that is the mean lifetime of QD PL is essentially larger that the energy transfer time. It means that the attachment of one extra-ligated $(L)ZnP^{4+}$ molecule on sulphur facet surface of AIS/ZnS/GSH QD leads to a strong (full practically) quenching of QD PL which may be caused by the fast FRET (in ps time scale). In the experiment, it manifests itself in the strong decrease of QD PL intensity without noticeable decay shortening of QD PL (at the given experimental excitation conditions).

In this respect, the main question is: in what extent namely FRET AIS/ZnS/GSH QD → $(L)ZnP^{4+}$ is fully responsible for QD PL quenching in nanoassemblies under study. Usually in the FRET case, the direct verification of the energy transfer process as a real reason of PL quenching is the quantitative comparison of the absorption spectra of the *D-A* system with its fluorescence excitation spectra detected presumably in the region of the *A* fluorescence band, thus the real estimation of the so-called sensitization effect.[5,50,105,119] Correspondingly,[50,105] if in the given *D*−*A* system in which 100% of FRET passes from *D* to *A*, the sum of the donor and acceptor extinction spectra should be the same as the sum of their excitation spectra, provided that both are normalized to unity at the *A* peak (thus both are unitless). The reason for normalizing to the *A* peak is that the magnitude of this peak in the excitation spectra is independent of the degree of FRET and serves as a reference for how much donor character, and thus FRET, is present in the *D-A* nanoassembly. Figure 8 shows a comparison of the normalized absorption and fluorescence excitation spectra for AIS/ZnS/GSH QD-$(L)ZnP^{4+}$ nanoassemblies at final titration step when QD PL is fully quenched.

The presented results show that in the spectral range of 280-370 nm (marked by blue doted line), corresponding to presumable absorption of QD with respect to porphyrin $(L)ZnP^{4+}$, curve 2 is relatively lower than curve 1 (nanoassembly absorption) but at the same time is higher noticeably than curve 3 in Figure 1 belonging to the absorption of alone $(L)ZnP^{4+}$. Based on these results, the estimated FRET efficiency corresponds to the value $\Phi_{FRET} \leq 0.6–0.65$. It follows from these data that FRET QD→porphyrin in the given nanoassemblies, may not be considered as one reason of QD PL quenching. Correspondingly, some other competitive non-radiative relaxation pathways may be responsible also for the QD PL quenching upon attachment of $(L)ZnP^{4+}$ molecule to the surface of AIS/ZnS/GSH QD.

Earlier it was quantitatively clarified[5,29,47,53,64,106,109] that for nanoassemblies based on TOPO-capped CdSe/ZnS QDs ($d_{CdSe} = 2.1–5.2$ nm) and coordinatively attached porphyrin molecules in non-polar toluene at ambient temperature, FRET transfer times between QDs and porphyrin molecules are in the range of 10–30 ns, and FRET efficiencies were measured to be $\Phi_{FRET} \approx 10–15\%$ from the QD PL total quenching. For the latter nanoassemblies, because of larger R_{DA} distances and smaller overlap integral $J(\nu)$ values, rate constants for FRET QD → porphyrin are smaller essentially compared to those found for AIS/ZnS/GSH QD-$(L)ZnP^{4+}$ nanoassemblies here. In addition, it was found that in nanoassemblies based on CdSe/ZnS QDs, namely competing non-FRET processes play a dominant role in the non-radiative relaxation of QD excited states. Based on quantitative comparison of experimental QD PL quenching rate constants with results of quantum mechanical calculations of the probability density $\Psi^2(r)$ corresponding to the quantum-confined *s*-type electronic wave function for a *1s* electron of the electron-hole pair of excited QD, it was argued[29,53,97,109,129] that in CdSe/ZnS QD-porphyrin nanoassemblies, non-FRET processes are caused by processes of electron (of the excited electron-hole pair) tunneling from CdSe core through the ZnS shell under conditions of quantum confinement as well by the influence of the ligand dynamics leading to the formation of surface trap states. It was found also, that the efficiency of non-FRET quenching depends on various factors, including QD size, the number of attachment sites, the microscopic nature of these sites, which might be additionally influenced by the solvent polarity, crystal structure (facets) and QD surface geometry.

In the case of AIS/ZnS/GSH QD-$(L)ZnP^{4+}$ nanoassemblies, effective FRET occurs in ps time scale. Nevertheless, the non-FRET quenching caused by electron tunnelling may still compete with the non-radiative FRET channel due to smaller QD size and closer displacement of the attached $(L)ZnP^{4+}$ macrocycle on sulphur facet surface of QD (i.e. electron tunnelling increase caused by stronger quantum confinement followed by effective trapping). In its turn, one single $(L)ZnP^{4+}$ molecule on the QD surface clearly resembles the tunneling of an electron (through the ZnS barrier) to the outer interface of the QD. Such tunneling is followed by the (self-) localization of the electron. This corresponds to the creation or modification of trap states in the semiconductor band gap. Such traps might be subject to non-radiative channels *e.g.* via enhanced electron-phonon coupling. Recently,[130] larger ternary spherical-shaped (d = 3.7−6.2 nm) Ag−In−Zn−S and Ag−In−S QDs were synthesized and characterized. Their PL spectra could be controllably tuned in the spectral range from 530 to 730 nm, PL quantum yield is 20−40%, and these Ag−In−S and Ag−In−Zn−S QDs exhibited the longest, reported to date, PL decays of ~9.4 and ~1.4 μs, respectively. These QDs may be considered as interesting candidates for the formation and study of larger QD-porphyrin nanoassemblies (containing more than one porphyrin molecule) as well as for testing of the proposed theoretical modelling of properties and surface morphology for larger QDs.

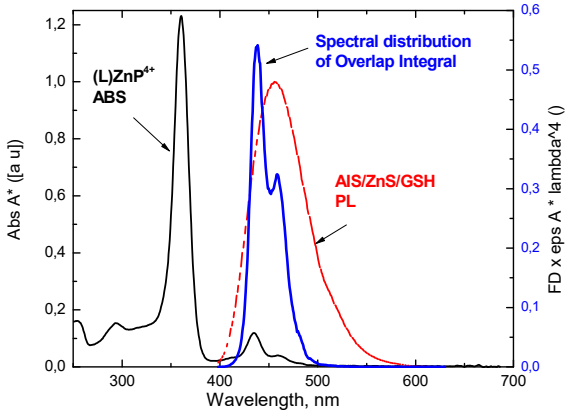

Figure 7. Spectral distribution of the overlap integral for *D*-*A* pair in nanoassembly AIS/ZnS/GSH QD - (L)ZnP^{4+}.

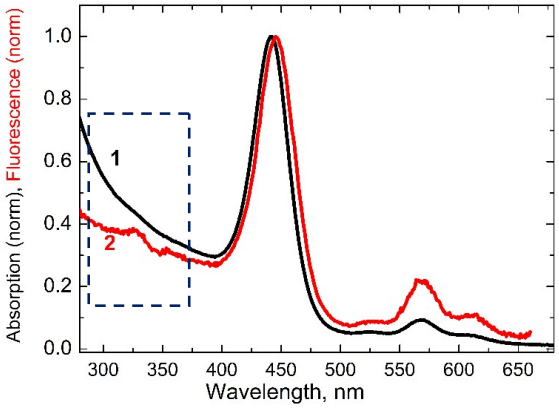

Figure 8. Normalized (with respect to the intensity of the porphyrin Soret band, λ_{max} =444 nm) absorption (1) and fluorescence excitation (2, λ_{reg} =680 nm) spectra for AIS/ZnS/GSH QD - (L)ZnP^{4+} nanoassemblies at final titration step (molar ratio $x \geq 1$, water, p*H* 7.5, T=298 K).

Conclusions

Qualitative and quantitative analysis of surface and interface processes in nanoassemblies based on semiconductor QDs and organic chromophores which may be tuned by tailoring the surface state energy and by varying the specific interactions with attached dye molecules is a key challenge for those working on hybrid nanomaterials and their applications. In this contribution, the results of the experimental studies and quantum chemical calculations are comparatively discussed for glutathione stabilized core/shell semiconductor AIS/ZnS/GSH quantum dots upon their electrostatic interactions with positively charged 5,10,15,20-tetra(N-methyl-4-pyridyl)porphyrin molecules in water at ambient temperature.

Based on steady-state absorption/photoluminescence, time-resolved photoluminescence (TCSPC), and Raman spectroscopy, interface phenomena, photoluminescence quenching as well as pathways and mechanisms of exciton relaxation in AIS/ZnS/GSH QD – porphyrin nanoassemblies are analysed. Using elaborated size-consistent quantum chemical atomistic 3D model for AIS/ZnS/GSH QD (based on method MM+), we propose a detailed physico-chemical description for the interaction of the porphyrin macrocycle with the glutathione capped QD. It includes electrostatic interactions of the positively charged porphyrin free base molecule with negatively charged capping ligand (glutathione), followed by a very fast metalation of porphyrin free base (formation of the axial aqua Zn-complex, $(H_2O)ZnP^{4+}$). It was shown that, spectral properties of attached Zn-porphyrin reflect the interaction of central Zn ion of the porphyrin macrocycle with a strong ligand on QD surface. It follows from the elaborated 3D model that in AIS/ZnS/GSH QD – porphyrin nanoassemblies, the tetracation ZnP^{4+} lies on the SH-facet surface, forming an axial coordination bond $(\equiv S^-)$-ZnP^{4+} between zinc ion in ZnP^{4+} and surface sulphur atom (manifesting a strong extra-ligation effect), accompanied by multiple ≡SH-π interactions, thus resulting in the final "guest" geometry via chemisorption (docking) of (L)ZnP^{4+} molecule on the SH facet.

Then, on the basis of the quantitative comparison of the results for the strong "quasi-static" quenching of QD PL and the fluorescence sensitization of attached (L)ZnP^{4+} molecule, it was evaluated that the dynamics and pathways of excitation energy relaxation processes in AIS/ZnS/GSH QD – porphyrin nanoassemblies are caused by two main competitive non-radiative processes, namely Förster resonance energy transfer AIS/ZnS/GSH QD → Zn-porphyrin (in ps time scale), and the electron tunnelling beyond the AIS/ZnS core under conditions of quantum confinement.

These studies demonstrate that the combination of experimental techniques and molecular-level insight into QD morphology may increase our molecular-level understanding of the surface chemistry and photophysical events in QD-dye nanoassemblies. Basic results being obtained and discussed here, may be useful in the directed formation of new nanoscale organic-inorganic building blocks and offer significant advantages in a wide areas of applications.

Acknowledgements. This work was supported by BSPSR program "Photonics and Electronics for Innovations (Belarus, 2021-2025)", RFBR grant 18-53-00035 (Russia-Belarus), Russian Science Foundation (Project 18-73-00234), as well as by the European Union under Grant Agreement 732482 in the framework of a Training Period (E.Z.), and Visiting Scholar Program of TU Chemnitz, Germany (E.Z., 2020-2021).

References

1. Lehn J.-M. *Angew. Chem., Int. Ed.* **1988**, *27*, 89–112.
2. Balzani V., Gómez-López M., Stoddart J.F. *Acc. Chem. Res.* **1998**, *31*, 405–414.
3. Livoreil A., Dietrich-Buchecker C.O., Sauvage J.-P. *J. Am. Chem. Soc.* **1994**, *116*, 9399–9400.
4. Krause S., Feringa B.L. *Nat. Rev. Chem.* **2020**, *4*, 550–562.
5. Zenkevich E., von Borczyskowski C. *Self-Assembled Organic-Inorganic Nanostructures: Optics and Dynamics.* Singapore: Pan Stanford. **2016**. 408 p.

6. Pochan D., Scherman O. *Chem. Rev.* **2021**, *121*, 13699–13700.
7. Jin Z., Dridi N., Palui G., Palomo V., Jokerst J.V., Dawson P.E., Amy Sang Q.-X., Mattoussi H. *Anal. Chem*. **2023**, *95*, 2713–2722.
8. Navalón S., Dhakshinamoorthy A., Álvaro M., Ferrer B., García H. *Chem. Rev*. **2023**, *123*, 445–490.
9. Zhong H., Wang M., Ghorbani-Asl M., Zhang J., Ly K.H., Liao Z., Chen G., Wei Y., Biswal B.P., Zschech E., Weidinger I.M., Krasheninnikov A.V., Dong R., Feng X. *J. Am. Chem. Soc*. **2021**, *143*, 19992−20000.
10. Ohta K. *Physics and Chemistry of Molecular Assemblies*. Singapore: World Scientific. **2020**.
11. Bertino M.F. *Introduction to Nanotechnology*. Singapore: World Scientific. **2021**.
12. Zhang X., Lu Y., Sun J., Liu Y., Dong H., Li C., Li Y., Jiang L. *ACS Materials Lett*. **2022**, *4*, 548−553.
13. Li D.J., Li Q.H., Gu Z.G., Zhang J. *Nano Lett*. **2021**, *21*, 10012−10018.
14. Enakieva Y.Y., Zhigileva E.A., Fitch A.N., Chernyshev V.V., Stenina I.A., Yaroslavtsev A.B., Sinelshchikova A.A., Kovalenko K.A., Gorbunova Y.G., Tsivadze A.Yu. *Dalton Trans.* **2021**, *50*, 6549–6560.
15. *Organic Nanophotonics (NATO Science Series II: Mathematics, Physics and Chemistry)* (Charra F., Agranovich V.M., Kajzar F., Eds.), New York: Academic Publishers, Kluwer, **2004**.
16. *Multiporphyrin Arrays: Fundamentals and Applications* (Kim D., Ed.), Singapore: Pan Stanford Publ. Pte. Ltd., **2012**. 775 p.
17. Zenkevich E.I., von Borczyskowski C. Multiporphyrin Self-Assembled Arrays in Solutions and Films: Thermodynamics, Spectroscopy and Photochemistry. In: *Handbook of Polyelectrolytes and Their Applications* (Tripathy S.K., Kumar J., Nalwa H.S., Eds.) USA: American Scientific Publishers, **2002**. Vol. 2, Ch. 11, pp. 301–348.
18. Fukuzumi S., Lee Y.M., Nam W. *ChemPhotoChem.* **2018**, *2*, 121–135.
19. Hood D., Sahin T., Parkes-Loach P.S., Jiao J., Harris Michelle A., Dilbeck P., Niedzwiedzki D.M., Kirmaier C., Loach P.A., Bocian D.F., Lindsey J.S., Holten D. *ChemPhotoChem.* **2018**, *2*, 300–313.
20. Wibmer L., Lourenco L.M.O., Roth A., Katsukis G., Neves M.G.P., Cavaleiro J.A.S., Tomé J.P.C., Torres T., Guldi D.M. *Nanoscale* **2015**, *7*, 5674–5682.
21. Biswas K., Urbani M., Sánchez-Grande A., Soler-Polo D., Lauwaet K., Matěj A., Mutombo P., Veis L., Brabec J., Pernal K., Gallego J.M., Miranda R., Écija D., Jelinek P., Torres T., Urgel J.I. *J. Am. Chem. Soc*. **2022**, *144*, 12725–12731.
22. Torres T., Bottari G. *Organic Nanomaterials: Synthesis, Characterization, and Device Applications*. John Wiley & Sons, **2013**. 632 p.
23. Jing H., Rong J., Taniguchi M., Lindsey J.S. *Coord. Chem. Rev.* **2022**, *456*, 214278.
24. Roy P.P., Kundu S., Valdiviezo J., Bullard G., Fletcher J.T., Liu R., Yang S.J., Zhang P., Beratan D.N., Therien M.J., Makri N., Fleming G.R. *J. Am. Chem. Soc.* **2022**, *144*, 6298–6310.
25. Cook L.P., Brewer G., Wong-Ng W. *Crystals* **2017**, *7*, 223–245.
26. Hirao T., Haino T. *J. Porphyrins Phthalocyanines* **2023**, *27*, 966–979.
27. Zvyagina A.I., Aleksandrov A.E., Martynov A.G., Kalinina M.A. *Inorg. Chem*. **2021**, *60*, 15509–15518.
28. Francesca S., Wennink J.W.H., Mäkinen P.I., Holappa L.P., Trohopoulus P.N., Ylä-Herttuala S., van Nostrum C., de la Escosura A., Torres T. *J. Mater. Chem. B*. **2020**, *8*, 282–289.
29. Koifman O.I., Ageeva T.A., Beletskaya I.P., Averin A.D., Yakushev A.A., Tomilova L.G., Dubinina T.V., Tsivadze A.Yu., Gorbunova Yu.G., Martynov A.G., Konarev D.V., Khasanov S.S., Lyubovskaya R.N., Lomova T.N., Korolev V.V., Zenkevich E.I., Blaudeck T. , Ch. von Borczyskowski, Zahn D.R.T., Mironov A.F., Bragina N.A., Ezhov A.V., Zhdanova K.A., Stuzhin P.A., Pakhomov G.L., Rusakova N.V., Semenishyn N.N., Smola S.S., Parfenyuk V.I., Vashurin A.S., Makarov S.V., Dereven'kov I.A., Mamardashvili N.Zh., Kurtikyan T.S., Martirosyan G.G., Burmistrov V.A., Aleksandriiskii V.V., Novikov I.V., Pritmov D.A., Grin M.A., Suvorov N.V., Tsigankov A.A., Fedorov A.Yu., Kuzmina N.S., Nyuchev A.V., Otvagin V.F., Kustov A.V., Belykh D.V., Berezin D.B., Solovieva A.B., Timashev P.S., Milaeva E.R., Gracheva Yu.A., Dodokhova M.A., Safronenko A.V., Shpakovsky D.B., Syrbu S.A., Gubarev Yu.A., Kiselev A.N., Koifman M.O., Lebedeva N.Sh., Yurina E.S. *Macroheterocycles* **2020**, *13*, 311–467.
30. He H., Lee S., Liu N., Zhang X., Wang Y., Lynch V.M., Kim D., Sessler J.L., Ke X.-S. *J. Am. Chem. Soc.* **2023**, *145*, 3047–3054.
31. Koifman O.I., Ageeva T.A., Kuzmina N.S., Otvagin V.F., Nyuchev A.V., Fedorov A.Yu., Belykh D.V., Lebedeva N.Sh., Yurina E.S., Syrbu S.A., Koifman M.O., Gubarev Y.A., Bunin D.A., Gorbunova Yu.G., Martynov A.G., Tsivadze A.Yu., Dudkin S.V., Lyubimtsev A.V., Maiorova L.A., Kishalova M.V., Petrova M.V., Sheinin V.B., Tyurin V.S., Zamilatskov I.A., Zenkevich E.I., Morshnev P.K., Berezin D.B., Drondel E.A., Kustov A.V., Pogorilyy V.A., Noev A.N., Eshtukova-Shcheglova E.A., Plotnikova E.A., Plyutinskaya A.D., Morozova N.B., Pankratov A.A., Grin M.A., Abramova O.B., Kozlovtseva E.A., Drozhzhina V.V., Filonenko E.V., Kaprin A.D., Ryabova A.V., Pominova D.V., Romanishkin I.D., Makarov V.I., Loschenov V.B., Zhdanova K.A., Ivantsova A.V., Bortnevskaya Yu.S., Bragina N.A., Solovieva A.B., Kuryanova A.S., Timashev P.S. *Macroheterocycles* **2022**, *15*, 207–302.
32. Matern J., Maisuls I., Strassert C.A., Fernández G. *Angew. Chem., Int. Ed*. **2022**, *61*, e2022084.
33. Yang F., Dong J., Li Z., Wang Z. *ACS Nano* **2023**, *17*, 4102–4133.
34. Ogawa T., Sinha N., Pfund B., Prescimone A., Wenger O.S. *J. Am. Chem. Soc*. **2022**, *144*, 21948–21960.
35. Ho-Yeung Chan M., Wing-Wah Yam V. *J. Am. Chem. Soc*. **2022**, *144*, 22805−22825.
36. Faraonov M., Martynov A.G., Polovkova M.A., Khasanov S.S., Gorbunova Yu.G., Tsivadze A.Yu., Otsuka A., Yamochi H., Kitagawa H., Konarev D.V. *Magnetochemistry* **2023**, *9*, 36.
37. Martynov A.G., Polovkova M.A., Gorbunova Yu.G., Tsivadze A.Yu. *Molecules* **2022**, *27*, 6498.
38. Efros A.L., Brus L.E. *ACS Nano* **2021**, *15*, 6192−6210.
39. Kovalenko M.V., Manna L., Cabot A., Hens Z., Talapin D.V., Kagan C.R., Klimov V.I., Rogach A.L., Reiss P., Milliron D.J., Guyot-Sionnest P., Konstantatos G., Parak W.J., Hyeon T., Korgel B.A., Murray C.B., Heiss W. *ACS Nano* **2015**, *9*, 1012–1057.
40. von Borczyskowski C., Zenkevich E. *Tuning Semiconduting and Metallic Quantum Dots: Spectroscopy and Dynamics.* Pan Stanford Publishing Pte. Ltd, **2017**. 398 p.
41. Wu N., Kirkwood N., Saker Neto N., Pervin R., Mulvaney P., Wong W.W.H. *J. Phys. Chem. C* **2023**, *127*, 2116–2126.
42. Cadena D.M., Sowa J.K., Cotton D.E., Wight C.D., Hoffman C.L., Wagner H.R., Boette J.T., Raulerson E.K., Iverson B.L., Rossky P.J., Roberts S.T. *J. Am. Chem. Soc.* **2022**, *144*, 22676−22688.
43. Zenkevich E.I., von Borczyskowski C. Formation Principles and Excited States Relaxation in Self-Assembled Complexes: Multiporphyrin Arrays and "Semiconductor CdSe/ZnS Quantum Dot-Porphyrin" Nanocomposites. In: *Handbook of Porphyrin Science with Application to Chemistry, Physics, Materials Science, Engineering, Biology and Medicine. Vol. 22 – Biophysical and Physicochemical Studies of Tetrapyrroles* (Kadish K., Smith K.M., Guilard R, Eds.), Singapore: World Scientific Publishing Co. Pte. Ltd, **2012**, 67–168.

44. Zenkevich E.I., Sagun E.I., Knyukshto V.N., Stasheuski A.S., Galievsky V.A., Stupak A.P., Blaudeck T., von Borczyskowski C. *J. Phys. Chem. C* **2011**, *115*, 21535–21545.
45. Sewid F.A., Annas K.I., Dubavik A., Veniaminov A.V., Maslov V.G., Orlova A.O. *RSC Adv.* **2022**, *12*, 899–906.
46. Rybkin A.Y., Belik A.Y., Goryachev N.S., Mikhaylov P.A., Kraevaya O.A., Filatova N.V., Parkhomenko I.I., Peregudov A.S., Terent'ev A.A., Larkina E.A., Mironov A.F., Troshin P.A., Kotelnikov A.I. *Dyes Pigm.* **2020**, *180*, 108411.
47. Zenkevich E., Blaudeck T., Sheinin V., Kulikova O., Selyshchev O., Dzhagan V., Koifman O., von Borczyskowski C., Zahn D.R.T. *J. Mol. Struct*. **2021**, *1244*, 131239.
48. Yu X.T., Sui S.Y., He Y.X., Yu C.H., Peng Q. *Biomater. Adv*. **2022**, *135*, 212725.
49. Martyanov T.P., Tovstun S.A., Vasil’ev S.G., Martyanova E.G., Spirin M.G., Kozlov A.V., Klimenko L.S., Brichkin S.B., Razumov V.F. *J. Nanopart. Res.* **2022**, *24*, 129.
50. Zenkevich E., Shulga A., Cichos F., Petrov E.P., Blaudeck T., von Borczyskowski C. *J. Phys. Chem. B* **2005**, *109*, 8679–8692.
51. Dayal S., Lou Y., Samis A.C.S., Berlin J.C., Kenney M.E., Burda C. *J. Am. Chem. Soc.* **2006**, *128*, 13974–13975.
52. Martynenko I.V., Orlova A.O., Maslov V.G., Baranov A.V., Fedorov A.V., Artemyev M. *Beilstein J. Nanotechnol*. **2013**, *4*, 895–902.
53. Stupak A., Blaudeck T., Zenkevich E., Krause S., von Borczyskowski C. *Phys. Chem. Chem. Phys*. **2018**, *20*, 18579–18600.
54. Shu Y.F., Lin X., Qin H.Y, Hu Z., Jin Y.Z., Peng X.G. *Angew. Chem. Int. Ed.* **2020**, *59*, 22312–22323.
55. Kaushik P. *Hybrid Nanocomposites: Fundamentals, Synthesis, and Applications*, 1st Edition, USA: Jenny Stanford Publishing, **2019**.
56. Kundu S., Patra A. *Chem. Rev*. **2017**, *117*, 712–757.
57. Calvin J., O’Brien E.A., Sedlak A.B., Balan A.D., Alivisatos A.P. *ACS Nano* **2021**, *15*, 1407–1420.
58. Saniepay M., Mi C., Liu Z., Abel E.P., Beaulac R. *J. Am. Chem. Soc*. **2018**, *140*, 1725−1736.
59. Chen Y., Smock S.R., Flintgruber A.H., Perras F.A., Brutchey R.L., Rossini A.J. *J. Am. Chem. Soc*. **2020**, *142*, 6117−6127.
60. Piveteau L., Morad V., Kovalenko M.V. *J. Am. Chem. Soc*. **2020**, *142*, 19413−19437.
61. Buckley J.J., Greaney M.J., Brutchey R.L. *Chem. Mater*. **2014**, *26*, 6311−6317.
62. Shen Y., Tan R., Gee M.Y., Greytak A.B. *ACS Nano* **2015**, *9*, 3345−3359.
63. Lee B., Littrell K., Sha Y., Shevchenko E.V. *J. Am. Chem. Soc*. **2019**, *141*, 16651−16662.
64. Kilin D.S., Tsemekham K., Zenkevich E.I., Prezhdo O.V., von Borczyskowski C. *J. Photochem. Photobiol. A* **2007**, *190*, 342–351.
65. Liu J., Kilina S., Tretiak S., Prezhdo O.V. *ACS Nano* **2015**, *9*, 9106–9116.
66. Kilina S.V., Tamukong P.K., Kilin D.S. *Acc. Chem. Res*. **2016**, *49*, 2127−2135.
67. Hartley C.L., Kessler M.L., Dempsey J.L. *J. Am. Chem. Soc*. **2021**, *143*, 1251–1266.
68. Du Fossé I., Lal S., Hossaini A.N., Infante I., Houtepen A.J. *J. Phys. Chem. C* **2021**, 125, 23968−23975.
69. Zito J., Infante I. *Acc. Chem. Res*. **2021**, *54*, 1555−1564.
70. Selyshchev O., Dzhagan V., Zenkevich E., Stroyuk O., Raievska O., Sheinin V., Kulikova O., Koifman O., Zahn D.R.T. Electronic interaction between Ag-In-S, Ag-In-S/ZnS quantum dots and quaternary amine aromatic molecules – a photoluminescence quenching study. In: *Book of Abstracts of the 14th Int. Symp. on Functional π-Electron Systems, Fπ14,* June 2–7, Berlin, **2019**, p. 106.
71. Sheinin V., Kulikova O., Zenkevich E., Selyshchev O., Dzhagan V., Stroyuk O., Raievska O., Koifman O., Zahn D.R.T. Tetra(N-methyl-4-pyridyl)porphyrin sonde report on the surface of AIS/ZnS/GSH quantum dots in water. In: *Book of Abstracts of the 1st Int. Conf. on Noncovalent Interactions, ICNI-2019*, 2–6 September, Lisbon, Portugal, **2019**, p. 82.
72. Zenkevich E., Sheinin V., Kulikova O., Selyshchev O., Dzhagan V., Stroyuk O., Raievska O., Koifman O., von Borczyskowski C., Zahn D.R.T. Self-assembled nano-composites based on semiconductor quantum dots and porphyrin molecules: interface chemistry, optical properties and energy relaxation processes. In: *Book of Abstracts of Webinar on Materials Science and Nanotechnology*. Coalesce Research Group, 33 Market Point Dr., Greenwille SC 29607, USA, July 29–30, **2020**, p. 11.
73. Motevich I.G., Zenkevich E.I., Stroyuk O.L., Raievska O.E., Kulikova O.M., Sheinin V.B., Koifman O.I., Zahn D.R.T., Strekal N.D. *J. Appl. Spectrosc*. **2020**, *87*, 926–935.
74. Zenkevich E., Sheinin V., Kulikova O., Koifman O. *Mathematical Methods in Technologies and Technique* **2022**, No. 11, 11–15.
75. Zenkevich E., Sheinin V., Kulikova O., Koifman O. *J. Porphyrins Phthalocyanines* **2023**, *27*, 19.
76. Zenkevich E., Sheinin V., Kulikova O., Koifman O. *J. Appl. Spectrosc*. **2023**, *90*, 18. [transl. *Zh. Prikl. Spektrosk.* **2023**, *90*(3), 434–446].
77. Sugata S., Yamanouchi S., Matsushima Y. *Chem. Pharm. Bull.* **1977**, *25*, 884–889.
78. Herrmann O., Mehdi S.H., Corsini A. *Can. J. Chem.* **1978**, *56*, 1084–1087.
79. Adler A.D., Longo F.R., Finarelli J.D., Goldmacher J., Assour J., Korsakoff L. *J. Organ. Chem.* **1967**, *32*, 476–476.
80. Hambright P., Gore T., Burton M. *Inorg. Chem.* **I976**, *15*, 2314–2315.
81. Sheinin V.B., Ivanov D.A., Koifman O.I. *Macroheterocycles* **2017**, *10*, 487–495.
82. Bailey S.L., Hambright P. *Inorg. React. Mech.* **2001**, *3*, 51–62
83. Raevskaya A., Lesnyak V., Haubold D., Dzhagan V., Stroyuk O., Gaponik N., Zahn D.R.T., Eychmüller A. *J. Phys. Chem. C* **2017**, *121*, 9032–9042.
84. Stroyuk O., Raevskaya A., Spranger F., Selyshchev O., Dzhagan V., Schulze S., Zahn D.R.T., Eychmüller A. *J. Phys. Chem. C* **2018**, *122*, 13648–13658.
85. Stroyuk O., Weigert F., Raevskaya A., Spranger F., Würth C., Resch-Genger U., Gaponik N., Zahn D.R.T. *J. Phys. Chem. C* **2019**, *123*, 2632–2641.
86. Sheinin V.B., Kulikova O.M., Lipatova I.M., Yusova A.A., Koifman O.I. *Dyes Pigm.* **2018**, *155*, 42–50.
87. Sheinin V.B., Kulikova O.M., Koifman O.I. *J. Mol. Liq.* **2019**, *277*, 397–408.
88. Boles M.A., Ling D., Hyeon T., Talapin D.V. *Nat. Mater*. **2016**, *15*, 141−153.
89. Ginterseder M., Franke D., Perkinson C.F., Wang L., Hansen E.C., Bawendi M.G. *J. Am. Chem. Soc*. **2020**, *142*, 4088−4092.
90. Giansante C. *J. Phys. Chem. C* **2018**, *122*, 18110−18116.
91. De Roo J., De Keukeleere K., Hens Z., Van Driessche I. *Dalton Trans*. **2016**, *45*, 13277−13283.
92. du Fossé I, ten Brinck S., Infante I., Houtepen A.J. *Chem. Mater*. **2019**, *31*, 4575−4583.
93. Krause M.M., Kambhampati P. *Phys. Chem. Chem. Phys*. **2015**, *17*, 18882−18894.
94. Duim H., Fang H.-H., Adjokatse S., ten Brink G.H., Marques M.A.L., Kooi B.J., Blake G.R., Botti S., Loi1 M.A. *Appl. Phys. Rev*. **2019**, *6*, 031401.
95. Zeng B., Palui G., Zhang C., Zhan N., Wang W., Ji X., Chen B., Mattoussi H. *Chem. Mater*. **2018**, *30*, 225−238.
96. Brown P.R., Kim D., Lunt R.R., Zhao N., Bawendi M.G., Grossman J.C., Bulovic V. *ACS Nano* **2014**, *8*, 5863–5872.
97. Blaudeck T., Zenkevich E.I., Abdel-Mottaleb M., Szwaykowska K., Kowerko D., Cichos F., von Borczyskowski C. *ChemPhysChem* **2012**, *13*, 959 – 972.
98. Zhong C., Sangwan V.K., Kang J., Luxa J., Sofer Z., Hersam M.C., Weiss E.A. *J. Phys. Chem. Lett*. **2019**, *10*, 493−499.

99. Lakowicz J. *Principles of Fluorescence Spectroscopy*. New York: Springer, **2006**.
100. Bellamy L.J. *The infra-red spectra of complex molecules* (3rd ed.) London: Chapman and Hall Ltd, **1975**.
101. Groenhof G. Introduction in QM/MM Simulations. In: *Biomolecular Simulations: Methods and Protocols, Methods in Molecular Biology* (Monticelli L., Salonen E., Eds.) New York: Springer Science+Business Media, **2013**, *924*, Ch. 3.
102. Hofer T.S., de Visser S.P. *Front. Chem*. **2018**, *6*, 367.
103. Tachiya M. *Chem. Phys. Lett*. **1975**, 33, 289–292.
104. Morris-Cohen A.J., Vasilenko V., Amin V.A., Reuter M.G., Weiss E.A. *ACS Nano* **2012**, *6*, 557–565.
105. Beane G., Boldt K., Kirkwood N., Mulvaney P. *J. Phys. Chem*. C **2014**, *118*, 18079−18086.
106. Zenkevich E., Von Borczyskowski C. Structural and Energetic Dynamics in Quantum Dot-Dye Nanoassemblies. In: *Self-Assembled Organic-Inorganic Nanostructures: Optics and Dynamics* (Zenkevich EI, von Borczyskowski C, Eds.) USA: Pan Stanford Publishing Pte. Ltd. **2016**, Chapter 4, pp 1–148.
107. Harris R.D., Bettis H.S., Kodaimati M., He C., Nepomnyashchii,A.B., Swenson N.K., Lian R., Calzada S., Weiss E.A. *Chem. Rev*. **2016**, *116*, 12865–12919.
108. Dworak L., Matylitzky V.V., Ren T., Basche T., Wachtveitl J. *J. Phys. Chem. C* **2014**, *118*, 4396–4402.
109. Zenkevich E., Stupak A., Göhler C., Krasselt C., von Borczyskowski C. *ACS Nano* **2015**, *9*, 2886–2903.
110. Zenkevich E.I., von Borczyskowski C. Photoinduced Relaxation Processes in Self-Assembled Nanostructures: Multiporphyrin Complexes and Composites “Cdse/Zns Quantum Dot-Porphyrin”. In: *Multiporphyrin Arrays: Fundamentals and Applications* (Kim D., Ed.) Singapore: Pan Stanford Publishing Pte. Ltd. **2012**. Ch. 5, pp. 217–288.
111. Sagun E.I., Zenkevich E.I., Knyukshto V.N., Shulga A.M., Starukhin D.A., von Borczyskowski C. *Chem. Phys*. **2002**, *275*, 211–237.
112. Knyukshto V.N., Sagun, E.I., Shulga A.M., Zenkevich, E.I. *J. Appl. Spectrosc*. **1998**, *65*, 900–907.
113. Zenkevich E.I., Chernook A.V., Shulga A.M., Sagun E.I., Gurinovich G.P. *Khimicheskaya Fizika* **1989**, *8*, 891–901.
114. Marcus R.A. *Rev. Modern Phys*. **1993**, *65*, 599–610.
115. Uno T., Koga M., Sotome H., Miyasaka H., Tamai N., Kobayashi Y. *J. Phys. Chem. Lett*. **2018**, *9*, 7098−7104.
116. Irgen-Gioro S., Yang M., Padgaonkar S., Chang W.J., Zhang Z., Nagasing B., Jiang Y., Weiss E.A. *Phys. Rev*. **2020**, *1*, 011305.
117. Förster T. *Modern Quantum Chemistry* (Sinanoglu O., Ed.), Academic Press: New York, **1965**.
118. Agranovich V.M., Galanin M.D. *Electronic Excitation Energy Transfer in Condensed Matter*. Amsterdam, New York: North-Holland Pub. Co. **1982**.
119. Clapp A.R., Medintz I.L., Uyeda H., Brent T., Fisher R., Goldman E.R., Bawendi M.G., Mattoussi H. *J. Am. Chem. Soc*. **2005**, *127*, 18212–18221.
120. Gerlach F., Täuber D., von Borczyskowski C. *Chem. Phys. Lett.* **2013**, *572*, 90–95.
121. Franceschetti A., Zunger A., Scholes G.D. *J. Phys. Chem. C* **2008**, *112*, 13336−13341.
122. Ray A., Bauri A., Bhattacharya S. *J. Mol. Liq.* **2018**, *263*, 64–71.
123. Hadar I., Halivni S., Even-Dar N., Faust A., Banin U. *J. Phys. Chem. C* **2015**, *119*, 3849−3856.
124. Funston A.M., Jasieniak J.J., Mulvaney P. *Adv. Mater*. **2008**, *20*, 4274–4280.
125. Padgaonkar S., Brown P.T., Jeong Y., Cherqui C., Avanaki K.N., López-Arteaga R., Irgen-Gioro S., Wu Y., Sangwan V.K., Schatz G.C., Hersam M.C., Weiss E.A. *J. Phys. Chem. C* **2021**, *125*, 15458−15464.
126. Basko D., La Rocca J.C., Bassani F., Agranovich V.M. *Eur. Phys. J. B* **1999**, *8*, 353–362.
127. Dmitriev O.P. *Chem. Rev.* **2022**, *122*, 8487–8593.
128. Atkins P., de Paula J. *Atkin's Physical Chemistry*. Oxford: Oxford University Press, **2002**. p. 577.
129. Blaudeck T., Zenkevich E., Cichos F., von Borczyskowski C. *J. Phys. Chem. C* **2008**, *112*, 20251–20257.
130. Kowalik P., Bujak P., Penkala M., Maroń A.M., Ostrowski A., Kmita A., Gajewska M., Lisowski W., Sobczak J.W., Pron A. *Chem. Mater*. **2022**, *34*, 809–825.

Received 17.04.2023
Accepted 10.05.2023